Synthetic and Systems Biotechnology 9 (2024) 549–557

Contents lists available at ScienceDirect

Synthetic and Systems Biotechnology

journal homepage: www.keaipublishing.com/en/journals/synthetic-and-systems-biotechnology

Original Research Article

Rational engineering of homospermidine synthase for enhanced catalytic efficiency toward spermidine synthesis

Wenjing Liu, Xiaoxiang Hu, Yi Yan, Yujie Cai *

The Key Laboratory of Industrial Biotechnology, Ministry of Education, School of Biotechnology, Jiangnan University, 1800 Lihu Road, Wuxi, Jiangsu, 214122, China

ARTICLE INFO

Keywords:
Homospermidine synthase
Polyamine
Site-directed mutagenesis
Spermidine
Structural analysis

ABSTRACT

Spermidine is a naturally occurring polyamine widely utilized in the prevention and treatment of various diseases. Current spermidine biosynthetic methods have problems such as low efficiency and complex multi-enzyme catalysis. Based on sequence-structure-function relationships, we engineered the widely studied homospermidine synthase from *Blastochloris viridis* (*Bv*HSS) and obtained mutants that could catalyze the production of spermidine from 1,3-diaminopropane and putrescine. The specific activities of *Bv*HSS and the mutants D361E and E232D + D361E (E232D-D) were 8.72, 46.04 and 48.30 U/mg, respectively. The optimal pH for both mutants was 9.0, and the optimal temperature was 50 °C. Molecular docking and dynamics simulations revealed that mutating aspartic acid at position 361 to glutamic acid narrowed the substrate binding pocket, promoting stable spermidine production. Conversely, mutating glutamic acid at position 232 to aspartic acid enlarged the substrate channel entrance, facilitating substrate entry into the active pocket and enhancing spermidine generation. In whole-cell catalysis lasting 6 h, D361E and E232D-D synthesized 725.3 and 933.5 mg/L of spermidine, respectively. This study offers a practical approach for single-enzyme catalyzed spermidine synthesis and sheds light on the crucial residues influencing homospermidine synthase catalytic activity in spermidine production.

1. Introduction

Biogenic amines (BAs) encompass a collection of aliphatic nitrogenous organic bases with low molecular weight that are ubiquitously found within the cellular composition of all living organisms. The compounds encompassed under this category consist of diamines (Fig. 1A) such as 1,3-diaminopropane (Dap), putrescine (Put), and cadaverine (Cad), as well as triamines (Fig. 1B) like spermidine (Spd) and homospermidine (Hspd) [1,2]. According to research, spermidine is an autophagy inducer with anti-aging properties [3]. In addition, a growing number of studies suggest that spermidine may play a beneficial role in the prevention and treatment of a variety of disorders, such as cardiovascular diseases [4], neurodegenerative pathologies [5], translation-associated disorders [6], and inflammation of liver fatty tissue [7]. Despite various research attempts to biosynthesis spermidine [8–11], the sustainable production of spermidine still confronts several problems, and it is desirable to develop new strategies for effective spermidine synthesis.

Homospermidine synthase (HSS, EC: 2.5.1.44), an NAD^+-dependent transferase, is responsible for transferring the aminobutyl group to putrescine. As early as 1979, Tait found that an HSS from *Blastochloris viridis* (*Bv*HSS) could catalyze two molecules of putrescine to produce one molecule of homospermidine [12]. Ober et al. noticed that *Bv*HSS also catalyze a number of side reactions, in the presence of a second substrate (such as Dap, Cad, or 1,6-diaminohexane), *Bv*HSS facilitates the reaction between putrescine and its analogous diamines, resulting in the production of both homospermidine and the corresponding N-(4-aminobutyl) derivatives (Fig. 1C) [13]. However, the catalytic efficiency of *Bv*HSS with 1,3-diaminopropane and putrescine as substrates is only 5 % compared to that with putrescine alone.

In recent years, protein engineering has emerged as a powerful strategy for obtaining target catalysts. Several studies have utilized molecular modification to successfully alter enzyme properties such as catalytic activity, stability, and selectivity [14–16]. *Bv*HSS consists of 477 amino acids, and its crystal structure has been identified as a dimer (Protein Data Bank [PDB] ID: 4PLP), with each monomer containing its own catalytically active center and NAD^+ binding site [17]. During the catalytic reaction facilitated by *Bv*HSS, the first putrescine molecule

Peer review under responsibility of KeAi Communications Co., Ltd.
* Corresponding author.
E-mail address: yjcai@jiangnan.edu.cn (Y. Cai).

https://doi.org/10.1016/j.synbio.2024.04.012
Received 13 December 2023; Received in revised form 10 April 2024; Accepted 11 April 2024
Available online 19 April 2024

entering the enzyme's active pocket undergoes oxidative deamination to form 4-aminobutanol, which then condenses with an amino group on the second putrescine molecule to form a Schiff base. This Schiff base is subsequently reduced to an imino group, resulting in the production of homospermidine. The entire catalytic process relies on the coordination among residues Asn-162, Trp-229, Glu-237, His-296, and the nicotine amide ring of NAD^+ [17,18]. 1,3-diaminopropane and putrescine share similar structural and physicochemical characteristics. The rational design of *Bv*HSS, guided by its structural features and catalytic mechanism, holds the promise of creating a mutant enzyme capable of catalyzing the reaction between 1,3-diaminopropane and putrescine to produce spermidine.

Whole-cell catalysis, as an enzyme catalysis method, streamlines the process by bypassing the need for isolating and purifying enzymes, thus cutting costs and simplifying operations [19]. In recent years, there has been a steady stream of research reports on the application of whole-cell catalysis [20,21]. Among these, *Escherichia coli* has emerged as the most favored host cell for whole-cell catalysis due to its simple structure and extensive research history [22,23].

In this study, we selected amino acid residues at the substrate binding pocket and substrate access tunnel for targeted mutation based on the 3D structures (PDB ID: 4TVB, 4XQC) and homologous sequence alignment of *Bv*HSS. Two mutants, namely D361E and D361E + E232D (referred to as E232D-D), were generated, displaying enhanced reaction rates for catalyzing 1,3-diaminopropane and putrescine. We extensively characterized the enzymatic properties of these mutants and elucidated the structural basis for the difference in catalytic ability compared to *Bv*HSS through molecular docking and molecular dynamics (MD) simulations. Furthermore, whole-cell catalysis was utilized to evaluate the production of spermidine by these mutants at different time intervals. Collectively, these findings lay the groundwork for the one-step enzyme-catalyzed production of spermidine.

2. Materials and methods

2.1. Materials

Ployamines and dansyl chloride were from Aladdin (Shanghai, China). NAD^+ was from Sangon Biotech (Shanghai, China). Kanamycin and isopropyl β-D-thiogalactoside were from Takara (Dalian, China). Enzymes used to clone, including 2 × FastPfu PCR SuperMix and 2 × FastTaq PCR SuperMix, were from Miozyme (Shanghai, China). QuickCut™ *Dpn* I were from Takara (Dalian, China). The AxyPrep Plasmid Miniprep Kit was from AXYGEN (Suzhou, China). All organic solvents were purchased from Sinopharm (Shanghai, China).

2.2. Preparation of recombinant BvHSS

The plasmid utilized in this study is pRSFDuet-1, which contains the homospermidine synthase gene (GenBank ID: MH192985) from *Blastochloris viridis* and was synthesized by Exsyn-bio Technology (Shanghai, China). The gene was inserted between the *Bam*H I and *Eco*R I sites of pRSFDuet-1 to obtain the recombinant plasmid pRSFDuet-*Bv*HSS, which was transformed into *Escherichia coli* (*E. coli*) JM109 for plasmid amplification and *E. coli* BL21 (DE3) for protein expression. The *E. coli* strains were cultured at 37 °C and induced for protein expression at 20 °C in Lysogenic Broth (LB) broth.

2.3. Site-directed mutagenesis of BvHSS

Primers for site-directed mutagenesis at various mutation sites were designed and are provided in Table S1. All primers were synthesized by Exsyn-bio Technology (Shanghai, China). A whole-plasmid PCR was performed using pRSFDuet-*Bv*HSS as a template. The PCR cycling program was set as follows: 94 °C, 2 min; 98 °C, 10 s, 56 °C, 10 s, and 72 °C, 1 min, (30 cycles); 72 °C, 5 min. The amplified PCR products were treated with restriction enzyme *Dpn* I at 37 °C during 3 h to eliminate the methylated template plasmid and then transformed into the competent *E. coli* JM109 cells using the heat-shock method. Multiple single colonies were selected and inoculated in an LB broth (containing 50 μg/mL kanamycin, K^+) for an overnight culture. The plasmids were extracted for DNA sequencing. Plasmids with correct mutations were retransformed by heat-shock transformation into the expression strain *E. coli* BL21 (DE3).

2.4. Recombinant protein expression and purification

Successful transformants were cultured in 50 mL of LB broth with 50 μg/mL K^+ until reaching an optical density at 600 nm (OD_{600}) between 0.4 and 0.8 units. Subsequently, induction was initiated by adding 0.4 mM isopropyl β-D-1-thiogalactopyranoside (IPTG) and incubating at 20 °C for 24 h. After incubation, cells were harvested by centrifugation at 8000×*g* for 5 min. The cell pellets were resuspended in 100 mM Tris-HCl buffer (pH 9), followed by cell lysis using sonication.

Purification of the overexpressed C-terminally 6 × His-tagged protein was performed using immobilized metal affinity chromatography (IMAC) with magnetic beads (BeaverBeads™ His-tag Protein Purification, Suzhou, China) according to the manufacturer's instructions. Briefly, a 10 mL sample was incubated with magnetic beads for 30 min. The impurities were then eluted using a solution of 100 mM Tris-HCl buffer (pH 9) containing 500 mM NaCl and 50 mM imidazole, while the recombinant protein was eluted with 100 mM Tris-HCl buffer (pH 9)

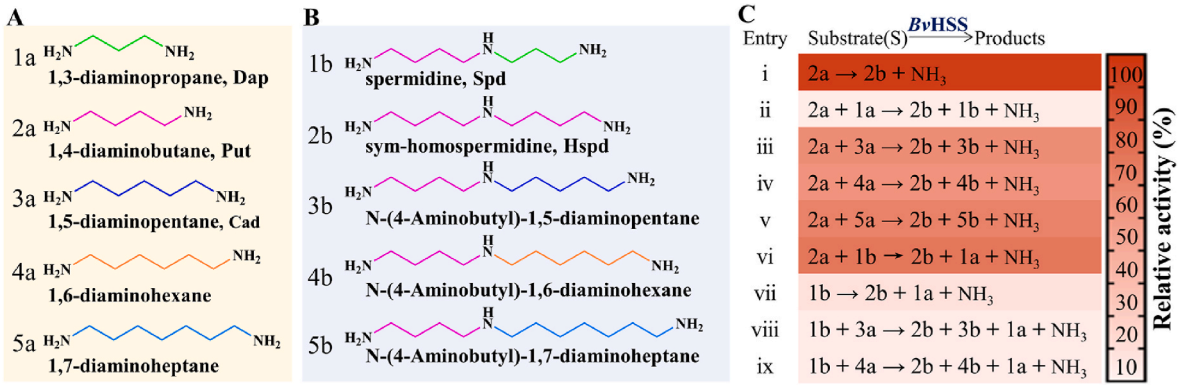

Fig. 1. Overview of *Blastochloris viridis* homospermidine synthase (*Bv*HSS)-related biogenic amines and the relative activities of *Bv*HSS-catalyzed reactions. (A) Two-dimensional structures of diamines. (B) Two-dimensional structures of triamines. (C) Comparison of the relative activities of known *Bv*HSS-catalyzed reactions. Relative activity is defined in terms of the amount of homospermidine (Hspd) produced by each reaction, where the enzyme-catalyzed 1,4-diaminobutane (Put) production of Hspd is 100 %.

containing 500 mM NaCl and 500 mM imidazole. The purified protein was desalted using a HiTrap desalting column (GE Healthcare) and stored at −80 °C. Additionally, the purity of all purified enzymes was confirmed by sodium dodecyl sulfate polyacrylamide gel electrophoresis (SDS-PAGE) analysis, and the protein concentration was determined using the Bradford Protein Assay Kit (Sangon Biotech, Shanghai, China).

2.5. Enzyme activity assay

The enzyme activity was determined following the method described by Krossa et al. [17]. The reaction was carried out in a total volume of 1 mL in 100 mM Tris-HCl buffer at pH 9, comprising 1 mM 1,3-diaminopropane and putrescine, 0.6 mM NAD^+, and an appropriate amount of enzyme solution. The mixture was incubated at 30 °C for 30 min. Following the assays, the system underwent derivatization and analysis by high-performance liquid chromatography (HPLC) to quantify the content of BAs. One unit (U) of enzyme activity is defined as the amount of enzyme required to convert 1 μmol of spermidine per minute under the given reaction conditions.

The method for detecting polyamines was comprehensively described by Liang et al. [24]. Standard solutions of spermidine were prepared with concentrations of 1.0 mg/L, 2.5 mg/L, 5.0 mg/L, 10.0 mg/L, 15.0 mg/L, 25.0 mg/L, and 50.0 mg/L to construct a standard curve (Fig. S1).

2.6. Determination of enzymatic properties, kinetic parameters, and substrate specificity

To assess the optimal pH conditions, buffers with varying pH levels were prepared, including phosphate buffer (pH 7.0–8.0, 100 mM), Tris-HCl buffer (pH 8.0–9.0, 100 mM), and Gly-NaOH buffer (pH 9.0–10.5, 100 mM) [25]. The reaction systems were exposed to different temperatures ranging from 30 °C to 60 °C to determine the optimum temperature. Additionally, the enzyme's thermostability was evaluated by measuring the residual activity after incubation at 50 °C for 2 h, 4 h, 6 h, 8 h, 10 h, and 12 h.

The kinetic parameters (K_M, V_{max}, k_{cat}, and k_{cat}/K_M) of *Bv*HSS and its mutants were determined and analyzed at 50 °C using a 100 mM Tris-HCl buffer (pH 9) supplemented with 0.6 mM NAD^+. Assays were determined at a varying concentration of substrate 1,3-diaminopropane (0.2, 0.4, 0.6, 0.8, 1.0, 1.2, 1.4, 1.6, 1.8, and 2.0 mM) with 2 mM putrescine or varied putrescine concentrations (0.2, 0.4, 0.6, 0.8, 1.0, 1.2, 1.4, 1.6, 1.8, and 2.0 mM) and 1 mM 1,3-diaminopropane. Enzyme activities corresponding to different substrate concentrations were calculated according to method 2.5. The K_M and V_{max} values were obtained by statistical analysis using the Graphpad Prism 8 software package (Graphpad Prism Software, San Diego, CA). The k_{cat} value was calculated using the equation $k_{cat} = V_{max}/(E)$, where (E) represents the molar concentration of the enzyme.

The substrate specificities of the wild-type (WT) and mutants were evaluated following the method described by Ober [13], using 1 mM BAs (including Dap, Put, Cad, 1,6-hexanediamine, and Spd) as substrates. The enzymes' substrate specificities were compared by quantifying the catalytically produced homospermidine.

2.7. Circular dichroism measurements

Circular dichroism spectra were acquired using a Jasco J720 spectropolarimeter (Jasco, Inc., Easton). Measurements were conducted with 200 μL of protein samples (0.2 mg/mL) in a 1 mm quartz cuvette containing 20 mM Tris-HCl buffer (pH 9.0). Spectra were recorded at 20 °C with a response time of 2 s, a path length of 0.1 cm, and a bandwidth of 2 nm across a wavelength range of 190–250 nm. Data were collected at intervals of 1 nm, and the scanning speed was set to 30 nm/min [26].

2.8. Structural analysis

The crystal structures of *Bv*HSS (PDB ID: 4PLP, 4TVB, 4XQC) were retrieved from the RSCB database, while homology modeling was carried out using AlphaFold2 [27]. Ligand structures for spermidine and homospermidine were sourced from PubChem. Molecular docking was performed using Autodock Vina [28], and the resulting structures were visualized using PyMOL software. Molecular dynamics simulations were conducted using Schrödinger Maestro Suite 2021-2, employing the OPLS4 force field for all computational steps [29]. Initially, the obtained complexes underwent preprocessing using the Protein Preparation Wizard module. Subsequently, all-atom dynamics simulations [30] spanning 300 ns were performed using Desmond, following the methodology outlined by Blake E. Smith et al. [31]. For the ensemble class, NPT was selected, with simulation temperatures set at 300 K or 323 K, and default parameters were applied. Throughout the simulations, coordinate frames were saved every 300 ps, resulting in a total of 1000 frames for subsequent analysis. The simulation interaction diagram tool was utilized to assess the Root Mean Square Deviation (RMSD) of Cα on the structure of each frame, as well as the Root Mean Square Fluctuation (RMSF) of amino acid fluctuations on the protein during the simulations [32].

2.9. Bioconversion of spermidine from 1,3-diaminopropane and putrescine

The reaction system was composed of 10 mL Tris-HCl buffer (100 mM, pH 9.0, 0.6 mM NAD^+, 40 g/L wet cells) with 10 mM 1,3-diaminopropane and putrescine. The reaction was performed at 50 °C for 6 h, and 100 μL of the reaction solution was withdrawn per hour, diluted to detect the content of polyamine.

2.10. Statistical analysis

Each experiment was conducted in triplicate, and the data are presented as mean values accompanied by standard deviations (SD). Error bars in the plots represent the SD.

3. Results

3.1. Mutation sites selection based on structure and sequence analysis

The crystal structure of *Bv*HSS, as described by Krossa et al. reveals that the enzyme's catalytic pocket resembles a "boot-shaped" cavity [17]. The catalytic residues are classified as inner, center, and outer amine sites, corresponding to the three amino groups on the product. As shown in Fig. 2B, *Bv*HSS residues E210 and D361 form hydrogen bonds with the N atom at homospermidine nitrogen 1 (inner amine site), while E237 forms a similar bond with the N atom at homospermidine nitrogen 11 (outer amine site). Additionally, N162 and W229 form hydrogen bonds and cation-π interactions with the N atom at homospermidine nitrogen 6 (center amine site) [18]. Spermidine shares a structural resemblance with homospermidine, featuring three amino groups and a carbon chain that is one methylene group shorter. To obtain a mutant enzyme capable of catalyzing spermidine synthesis, our initial consideration was to narrow the catalytic pocket. Given the documented inactivity of mutants E237Q, E210Q, E210A, and E210K in previous studies [17,18], and the high evolutionary conservation of residues E237 and E210, we initially opted to perform site-saturation mutagenesis at D361.

Co-crystallization of *Bv*HSS with 1,3-diaminopropane and putrescine (PDB ID: 4XQC) showed that two 1,3-diaminopropane molecules bind to *Bv*HSS, one at the active center and the other at the entrance to the active pocket [17]. As seen in Fig. 2C, the pink sticks are the six amino acids at the entrance of the active pocket of *Bv*HSS, among which E117 and E232 form interactions with the amino groups of 1,

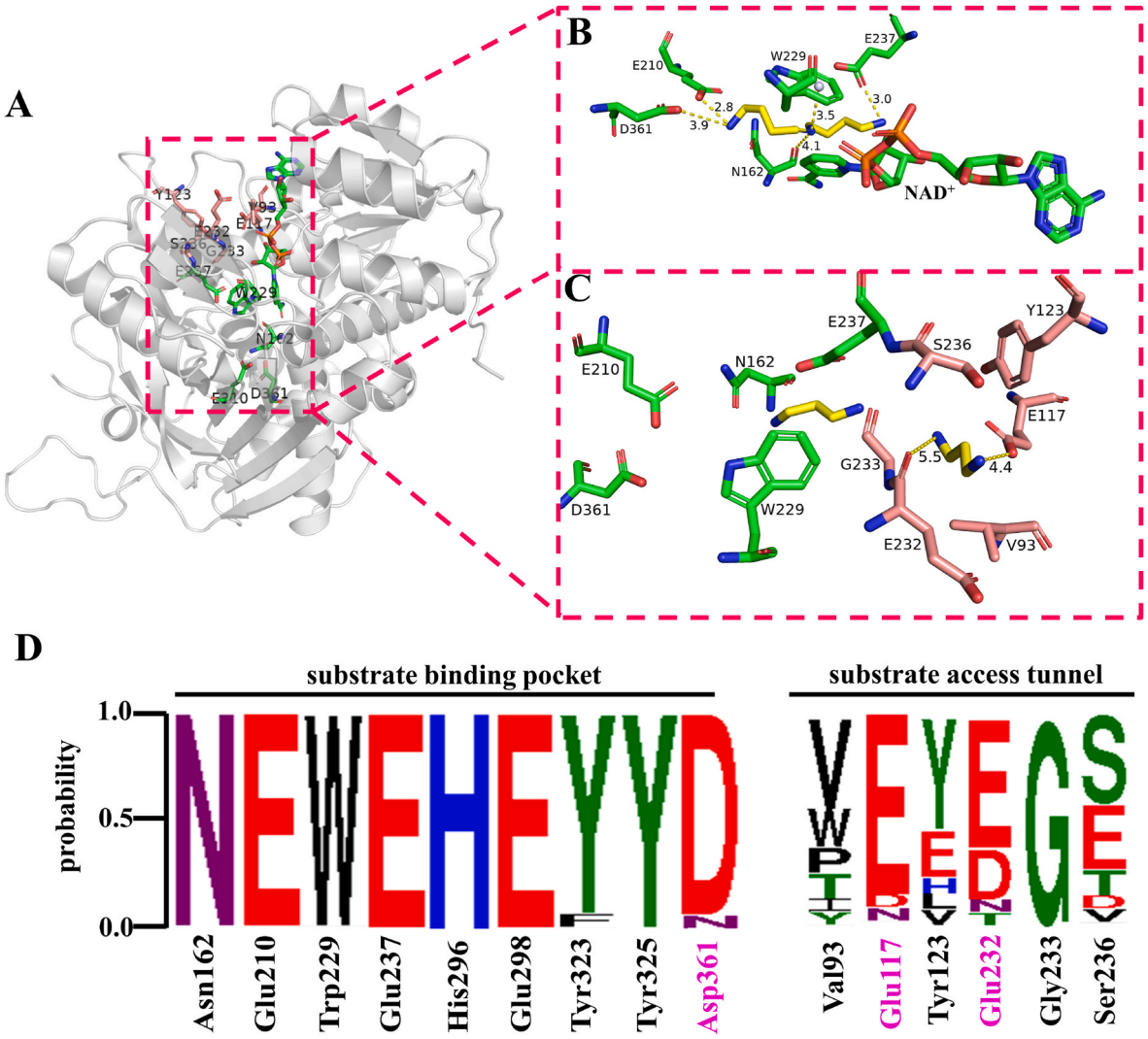

Fig. 2. Complex structure analysis and the conservation of active residues of the *Blastochloris viridis* homospermidine synthase (*Bv*HSS). (A) An overview of *Bv*HSS monomer (Protein Data Bank (PDB) ID: 4PLP), (B) Enlarged display of *Bv*HSS-homospermidine catalytic pocket (PDB ID: 4TVB), (C) Enlarged presentation of *Bv*HSS-1,3-diaminopropane (Dap) catalytic sites and ligand entrance tunnel (PDB ID: 4XQC). The magenta square emphasizes the location of the active pocket. The green sticks are catalytic residues, the pink sticks are the six amino acid residues at the entrance tunnel, the yellow sticks are ligands, and the yellow dashed line measures the distance between ligands and residues. (D) Sequence logo depicting the conservation of active residues. The three mutated amino acids are marked in pink. The sequence logo was generated using the program WebLogo.

3-diaminopropane, respectively. To prevent any potential impact on enzyme catalytic activity caused by the binding of 1,3-diaminopropane (Dap) at the substrate channel entrance, we focused on two residues, E117 and E232, known to interact with 1,3-diaminopropane. Based on homologous sequence comparisons (Fig. 2D and S2), we designed and constructed five single-point mutants (E117D, E117 N, E232D, E232 N, and E232T).

3.2. Enzyme activity assay

The catalytic activity of both the wild-type (WT) and mutants was measured using 1,3-diaminopropane and putrescine as substrates. According to Fig. 3, the enzyme activity of WT was 8.72 U/mg, while the D361E mutant exhibited a higher activity of 46.04 U/mg. Mutants D361A and D361T demonstrated activities of 15.36 U/mg and 9.63 U/mg, respectively, indicating a slight increase compared to the WT. On the other hand, mutants D361S, D361L, D361I, and D361V exhibited slightly lower activity than the WT, while other single-point mutants at this site did not enhance the reaction of 1,3-diaminopropane and putrescine (Fig. S3). For mutations at positions 117 and 232, the enzyme

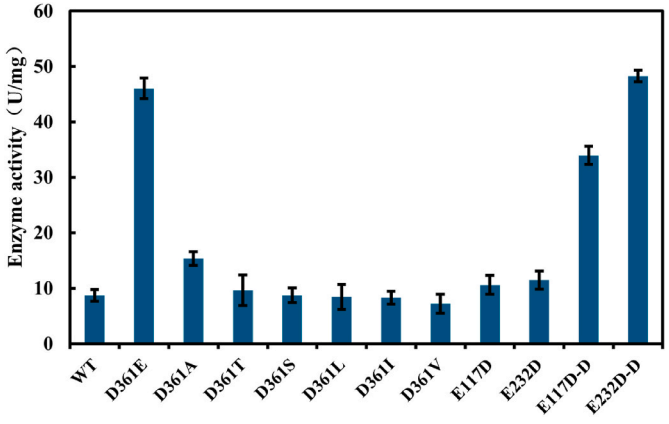

Fig. 3. Catalytic activities of wild-type (WT) and some variants. Other inactive mutants were not shown. All measurements were performed in triplicate, and the data are displayed as mean ± s.d.

activities of E117D and E232D were 10.57 and 11.46 U/mg, respectively, slightly higher than the WT (Fig. 3). However, E117 N, E232 N, and E232T were inactive, indicating that two acidic amino acids are required at the entrance of the substrate channel for the reaction. We conducted combinatorial mutagenesis of amino acids at positions 117, 232, and 361 to explore the collective impact of residues at the substrate binding pocket and substrate access tunnel on enzyme activity.

Using D361E as a template, we obtained the double-point mutants D361E + E117D (abbreviated as E117D-D) and D361E + E232D (abbreviated as E232D-D) by mutating glutamate to aspartate at positions 117 and 232. Compared to D361E, the enzyme activity of E117D-D decreased to 33.94 U/mg, while that of E232D-D increased to 48.30 U/mg. However, the three-point mutant D361E + E117D + E232D was found to be inactive.

3.3. Biochemical characterization of WT and D361E, E232D-D

The WT, D361E, and E232D-D proteins were expressed in soluble form, each exhibiting a molecular weight of 52 kDa (Fig. S4A). The catalytic reaction was evaluated using 1,3-diaminopropane and putrescine as substrates, with the corresponding HPLC profile is depicted in Fig. S4B. 1,7-diaminoheptane served as the internal standard, and enzyme activity was quantified based on the standard curve.

The specific activities of the three proteins showed an initial increase followed by a decrease with pH, reaching a peak at pH 9, as illustrated in Fig. 4A. Similarly, their activities followed a similar trend with temperature, increasing up to 50 °C before declining, as shown in Fig. 4B. Although both mutants shared the same optimal temperature for reaction as the wild type, they exhibited higher specific activity. Between 30 and 45 °C, the activities of D361E and E232D-D were comparable, with E232D-D exhibiting a 14.4 % increase over D361E at 50 °C. Both mutants maintained approximately 90 % activity at 55 °C, which sharply declined at 60 °C. Thermostability assessments revealed that all three enzymes exhibited favorable stability, retaining over 50 % catalytic activity after exposure to 50 °C for 4 h, as shown in Fig. 4C. This information can assist in determining the suitable time for enzyme catalysis reaction.

3.4. Kinetic characterization of WT and D361E, E232D-D

The kinetic properties of the enzymes were precisely determined by reactions with varied 1,3-diaminopropane concentrations while fixing putrescine concentration and varied putrescine concentrations while fixing 1,3-diaminopropane concentration. As shown in Table 1, the K_m of *Bv*HSS, D361E, and E232D-D for 1,3-diaminopropane were 0.49, 0.43, and 0.31 mM, respectively. Conversely, the K_m values of the three enzymes for putrescine were 0.51, 0.49, and 0.45 mM, respectively. Overall, the binding affinity between mutants and substrates was greater than that of WT. In contrast, the differences between the k_{cat} of the three enzymes were more obvious. For 1,3-diaminopropane and putrescine, respectively, the k_{cat} values of *Bv*HSS, D361E, and E232D-D were 13.64, 19.33, and 21.09 s^{-1} and 14.50, 21.90, and 25.92 s^{-1}. For 1,3-diaminopropane and putrescine, respectively, the k_{cat}/K_m values of *Bv*HSS, D361E, and E232D-D were 27.84, 44.95, and 68.03 $mM^{-1}s^{-1}$ and 28.43, 44.69, and 57.60 $mM^{-1}s^{-1}$. The results show that for 1,3-diaminopropane and putrescine, respectively, D361E and E232D-D were 1.62 and 2.44 times more efficient than WT. Both variants exhibit greater catalytic activity in the reaction between 1,3-diaminopropane and putrescine compared to *Bv*HSS.

Table 1
Kinetic parameters of the WT, D361E and E232D-D.

Substrate	enzyme	K_M (mM)	k_{cat} (s^{-1})	k_{cat}/K_M ($mM^{-1}s^{-1}$)
Dap	WT	0.49 ± 0.03	13.64 ± 0.37	27.84 ± 0.76
	D361E	0.43 ± 0.06	19.33 ± 0.92	44.95 ± 2.17
	E232D-D	0.31 ± 0.02	21.09 ± 0.74	68.03 ± 2.38
Put	WT	0.51 ± 0.05	14.50 ± 0.49	28.43 ± 2.43
	D361E	0.49 ± 0.04	21.90 ± 0.03	44.69 ± 2.56
	E232D-D	0.45 ± 0.02	25.92 ± 0.20	57.60 ± 2.03

3.5. Substrate specificity of WT and D361E, E232D-D

The reported optimal reaction temperature for the catalytic generation of homospermidine by *Bv*HSS in the literature is approximately 30 °C [33,34]. However, our experimental results suggest that 50 °C is more conducive to spermidine generation. Therefore, we evaluated the substrate specificity of WT and two mutants at both 30 °C and 50 °C. Since *Bv*HSS produces the same product, homospermidine, regardless of the substrate used, we quantified the relative activity based on the amount of homospermidine produced, as detailed in Table 2.

Table 2 shows that at 30 °C, the mutants exhibit homospermidine production from putrescine comparable to WT. However, at 50 °C, the activity of the three enzymes producing homospermidine from putrescine decreased. Neither WT nor the mutants catalyze the reaction using 1,3-diaminopropane or cadaverine as the sole substrate at any temperature (not shown in Table 2), consistent with previous reports [13]. When putrescine and 1,3-diaminopropane serve as substrates, the activity of *Bv*HSS is notably inhibited at 30 °C. However, at 50 °C, the *Bv*HSS-catalyzed production of homospermidine and Spd increases by 1.4 and 3.9 folds, respectively. The D361E mutant increases by 1.5 and 2.8 folds, while the E232D-D mutant increases by 1.6 and 3.4 folds under the same conditions. When using putrescine and Cad or 1,6-Diaminohexane as substrates, the two mutants catalyze the production of homospermidine less efficiently than WT at 30 °C, but produce N-(4-Aminobutyl)-1,5-diaminopentane and N-(4-Aminobutyl)-1,6-diaminohexane more than WT. Nonetheless, both mutants exhibit higher

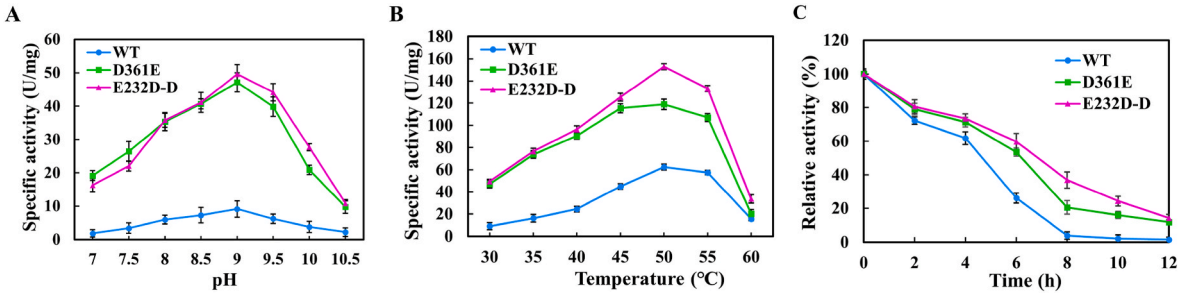

Fig. 4. Enzymatic properties of wild-type (WT) and its variants. Effects of pH (A) and temperature (B) on the activity of WT, D361E, and D361E + E232D (E232D-D). (C) Thermostability of WT, D361E, and E232D-D at 50 °C.

Table 2
Substrate specificity of the WT, D361E and E232D-D.

S[a]	P[b]	Relative activity (%)[c]					
		30 °C			50 °C		
		WT	D361E	E232D-D	WT	D361E	E232D-D
2a	2b	100.00	102.79	107.48	69.65	78.30	81.49
2a+1a	2b	5.09	38.15	31.05	12.22	58.24	50.02
	1b	2.18	14.40	13.47	10.76	40.85	45.94
2a+3a	2b	60.99	36.10	46.08	32.65	56.58	57.05
	3b	25.45	28.25	44.47	25.67	33.68	38.97
2a+4a	2b	67.77	58.22	40.80	43.62	50.44	56.81
	4b	29.40	35.82	37.09	30.82	37.11	40.94
2a+1b	2b	71.26	75.41	79.89	62.32	76.42	80.47
	1a	8.16	13.91	22.59	9.06	23.06	25.62
1b	2b	10.03	14.71	16.19	9.41	13.24	15.06
	1a	15.13	21.58	28.21	19.89	20.92	21.88
1b+3a	2b	14.59	19.96	18.13	9.94	12.88	11.69
	3b	20.73	24.07	25.63	31.14	36.90	37.49
	1a	17.66	31.37	29.80	23.76	35.32	39.18
1b+4a	2b	17.15	25.42	36.47	8.91	10.19	19.72
	4b	10.34	23.65	25.70	16.07	35.97	43.76
	1a	19.01	28.38	29.22	24.17	23.05	37.62

[a] S: Substrate(s).
[b] P: Product(s). Include 2a = Putrescine (Put); 1a = 1,3-Diaminopropane (Dap); 3a = 1,5-Diaminopentane (Cad); 4a = 1,6-Diaminohexane; 1b = Spermidine (Spd); 2b = Homospermidine (Hspd); 3b = *N*-(4-Aminobutyl)-1,5-diaminopentane; 4b = *N*-(4-Aminobutyl)-1,6-diaminohexane. Relative activity (%).
[c] Relative activity is defined in terms of the amount of homospermidine (Hspd) produced by each reaction, where the enzyme-catalyzed Put production of Hspd is 100 %.

catalytic activity in the synthesis of homospermidine and its N-(4-aminobutyl)-derivatives compared to WT at 50 °C. When Spd and putrescine were used as substrates, all three enzymes catalyzed the generation of homospermidine to more than 60 % of the control. However, when Spd or Spd with Cad or 1,6-Diaminohexane were used as substrates, all three enzymes exhibited limited catalytic capabilities.

3.6. Structural analysis and MD simulation

To comprehend the structural underpinnings of the enzyme's altered catalytic capacity, we utilized circular dichroism to analyze the secondary structure of both the WT and its mutants. As depicted in Fig. S5, the spectral trends of WT and mutants are highly similar, with slight changes observed in their secondary structures. Additionally, we computationally predicted the three-dimensional structures of D361E and E232D-D using AlphaFold2. Utilizing parKVFinder [35], we detected the cavities of WT, D361E, and E232D-D separately, and calculated the volumes of the active binding pockets. The volumes of the active binding pockets for the three enzymes were determined to be 304.34, 270.43, and 267.41 Å^3, respectively. We observed that the mutation of aspartic acid at position 361 to glutamic acid effectively reduced the volume of the binding pocket. Subsequently, each protein structure was semi-flexibly docked with spermidine to obtain the composite structure. In the docked WT-Spd complex structure (Fig. 5C), spermidine is positioned at distances of 3.4 Å, 2.5 Å, and 4.3 Å from the acidic amino acids E237, E210, and D361, respectively. In the D361E-Spd complex structure (Fig. 5D), these distances decrease to 2.8 Å, 2.7 Å, and 3.2 Å, respectively. Similarly, in the E232D-D-Spd complex structure (Fig. 5E), the distances are 3.0 Å, 3.0 Å, and 3.1 Å, respectively. This suggests that replacing aspartic acid with glutamic acid at position 361 in *Bv*HSS reduces the size of the substrate binding pocket, thereby shortening the distance between residue 361 and the substrate during catalysis and stabilizing the reaction product to some extent. The mutation of glutamic acid to aspartic acid at position 232 resulted in an increase in distance between this site and E117 from the original 6.2 Å to 7.0 Å. This change may contribute to the enhanced activity of the E232D-D mutant by facilitating easier entry of the substrate into the catalytic center, thereby leading to a faster reaction rate compared to before the mutation.

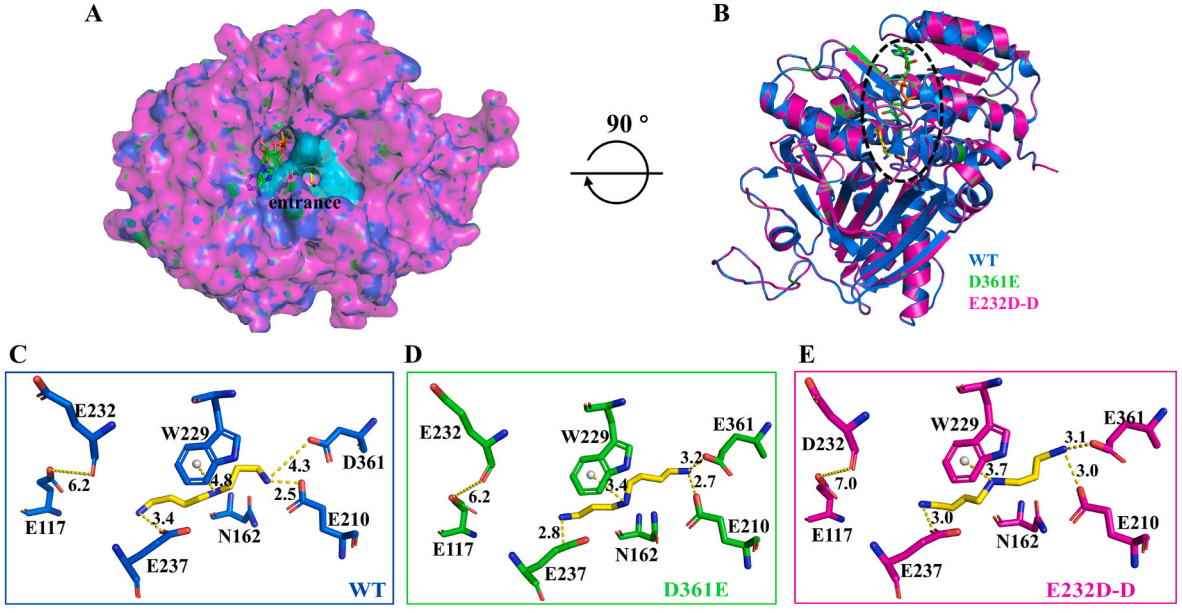

Fig. 5. Molecular docking analysis of *Blastochloris viridis* homospermidine synthase (*Bv*HSS) and its variants with spermidine. (A) Surface display of WT and mutant structures after superimposition. The small hole formed in the blue area is the entrance to the substrate channel. (B) Cartoon display after turning 90° upward in (A). Blue represents WT, green represents D361E, and pink represents D361E + E232D (E232D-D). (C–E) Detailed structure of WT, D361E, and E232D-D catalytic centers. The yellow sticks are spermidine and the yellow dashed line measures the distance between ligands and residues.

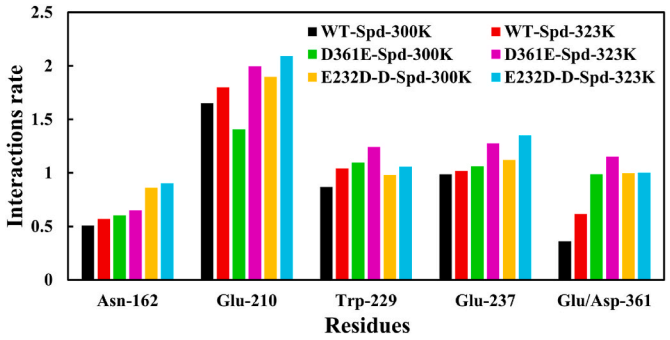

Fig. 6. The interaction rate exists between the ligand and conserved residues.

To verify the accuracy of the docking results, we conducted 300 ns MD simulations on the three complex structures at 300 K and 323 K. The RMSD fluctuations of the Cα atoms obtained during the simulations ranged from 1 to 3 Å (Fig. S6), indicating the reliability of the docking results. The RMSF shows the atomic fluctuations averaged on each protein residue during MD simulation [36]. Compared to 300 K, the complexes exhibited greater flexibility among conserved residues at 323 K (Fig. S7). Based on the observed catalytic activities at different temperatures, it is hypothesized that elevating the temperature will induce more pronounced conformational alterations in the enzyme catalyst. However, it is important to note that this expanded range of conformational changes is not conducive to the production of homospermidine but rather facilitates the reactions involving 1,3-diaminopropane and putrescine.

Fig. 6 illustrates the interaction forces between catalytic residues and spermidine, calculated by summing the strengths of hydrogen bonds, cation-π, and salt-bridge interactions. During the simulation at 300 K, the interaction forces between spermidine and *Bv*HSS are weakest in the WT-Spd complex. It was observed that the E232D-D-Spd complex exhibits the strongest interaction force during simulation at 323 K. A stronger interaction force between the enzyme and the ligand generally favors the enzyme-catalyzed reaction [37]. While the catalytic reaction of *Bv*HSS with 1,3-diaminopropane and putrescine substrates is limited at 30 °C, an increase in temperature to 50 °C enhances the interaction force between active residues and the ligand, consequently boosting enzyme activity. Similarly, point mutations induce structural changes that enhance the interaction force, thereby promoting the reaction between 1,3-diaminopropane and putrescine.

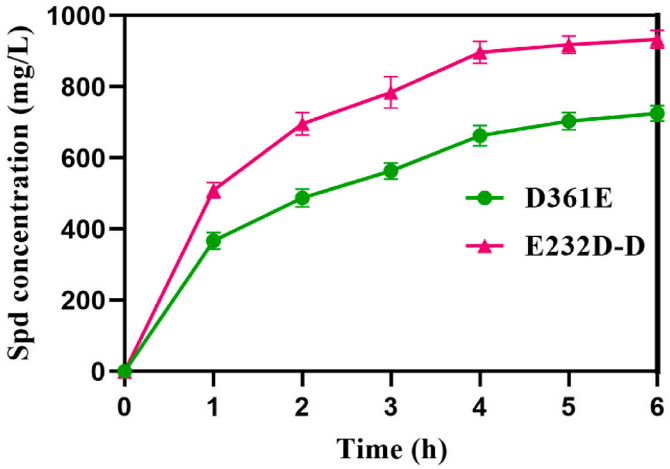

Fig. 7. Spermidine production by whole-cell catalyst of D361E and E232D-D.

3.7. Whole-cell catalytic synthesis of spermidine

The production of spermidine by D361E and E232D-D with whole cells was investigated. As illustrated in Fig. 7, the reaction lasted for 6 h using 10 mM of 1,3-diaminopropane and putrescine as substrates. E232D-D exhibited a higher catalytic activity for spermidine generation compared to D361E. The fastest accumulation of the product generation was found in the first hour, and after 4 h of the reaction, the amount of spermidine appeared to have stabilized and ceased to increase substantially. At the end of the 6 h reaction, D361E and E232D-D produced 725.3 mg/L and 933.5 mg/L of spermidine, respectively. The substrate conversion rates for D361E and E232D-D were 24.95 % and 32.15 %, respectively. The existing rate of substrate conversion is unsatisfactory, necessitating additional directed evolution of the enzymes to acquire mutants with enhanced catalytic efficiency.

4. Discussion

Spermidine is essential for maintaining human health and is involved in various disease processes [3]. Currently, commercially available spermidine is primarily obtained from plant extracts. Therefore, it is imperative to develop environmentally friendly and sustainable methods for its production [38]. Several studies have focused on devising synthetic routes for spermidine using metabolic engineering techniques that leverage the natural pathway for spermidine synthesis [8–10]. However, the complex coordination among the enzymes involved in this pathway has posed significant challenges for industrial spermidine production. The proposed single-step enzymatic spermidine synthesis is a simple and efficient method that could establish a novel pathway for spermidine biosynthesis. In this study, we employed a rational design approach based on structural and sequence analysis of *Bv*HSS and screened for mutants with enhanced spermidine production activity. We analyzed the enzymatic properties of *Bv*HSS and its mutants to compare their catalytic abilities and elucidate the enhanced activity of the mutants in relation to their three-dimensional structure. Additionally, we provisionally assessed the mutants' ability to facilitate spermidine production using whole-cell catalytic tests. This research could also serve as a valuable reference for the industrial-scale production of spermidine.

Firstly, the catalytic residues of *Bv*HSS influence its catalytic activity, as the amino groups of substrates are positively charged in alkaline solutions, facilitating interaction forces with negatively charged amino acids [39]. The active pocket of *Bv*HSS contains three acidic residues. When the amino acid residue D361 is mutated to glutamate, which has a longer carbon chain, the catalytic pocket shortens by approximately a methylene distance. This mutation, D361E, accelerates the reaction between 1,3-diaminopropane and putrescine 6.6-fold compared to WT. Conversely, mutating aspartate at position 361 to other amino acids mostly leads to enzyme inactivation, highlighting the importance of acidic amino acids in *Bv*HSS catalysis, consistent with other polyamine metabolism-related enzymes [40–42].

Secondly, the enzyme's catalytic activity is influenced by reaction temperature. The catalytic process of *Bv*HSS involves hydride transfer, which is temperature-sensitive [43]. When 1,3-diaminopropan and putrescine were used as substrates, the catalytic efficiency of *Bv*HSS was higher at 50 °C compared to 30 °C. This temperature-dependent trend in catalytic ability was also observed in the two mutants. MD simulations further revealed that the enzyme's conformation varied during the catalytic reaction at different temperatures. Notably, the conformational changes at higher temperatures were not conducive to homospermidine production but rather promoted the reactions leading to spermidine from 1,3-diaminopropane and putrescine.

Compared to pure microbial fermentation, whole-cell catalysis is simpler, has a shorter cycle, does not involve complex cellular metabolic pathways, yields more uniform products, and is more convenient for subsequent separation and purification. Although the current

spermidine conversion rate of whole-cell catalysis is not ideal, we believe that with the continuous development of protein molecular modification technology, obtaining efficient target catalysts through enzyme engineering in the future is promising.

5. Conclusion

In summary, we utilized a rational approach involving structural analysis of *Bv*HSS and alignments with homologous sequences to generate two mutants: D361E and E232D-D. These mutants effectively catalyze the conversion of 1,3-diaminopropane and putrescine into spermidine. By comparing the enzymatic characteristics and substrate specificity of *Bv*HSS and its mutants, it is evident that the HSS-catalyzed process is influenced by both mutation and elevated temperature. These findings serve as a theoretical foundation for future enzyme engineering studies related to polyamine metabolism. Our work presents a novel enzymatic synthesis pathway for spermidine. With advancements in directed evolution technology for enzymes, there is increasing potential to tailor enzyme molecules to specific reactions. This opens up possibilities for the development of innovative catalysts to facilitate the generation of spermidine from 1,3-diaminopropane and putrescine in the future.

Funding

This research did not receive any specific grant from funding agencies in the public, commercial, or not-for-profit sectors.

CRediT authorship contribution statement

Wenjing Liu: Conceptualization, Methodology, Data curation, Writing – original draft. **Xiaoxiang Hu:** Validation, Investigation. **Yi Yan:** Methodology, Formal analysis. **Yujie Cai:** Supervision, Project administration.

Declaration of competing interest

The authors declare that they have no known competing financial interests or personal relationships that could have appeared to influence the work reported in this paper.

Appendix A. Supplementary data

Supplementary data to this article can be found online at https://doi.org/10.1016/j.synbio.2024.04.012.

References

[1] Michael AJ. Polyamines in eukaryotes, bacteria, and archaea. J Biol Chem 2016;291(29):14896–903. https://doi.org/10.1074/jbc.R116.734780.
[2] Michael AJ. Biosynthesis of polyamines and polyamine-containing molecules. Biochem J 2016;473(15):2315–29. https://doi.org/10.1042/BCJ20160185.
[3] Madeo F, Eisenberg T, Pietrocola F, Kroemer G. Spermidine in health and disease. Science 2018;359(6374):eaan2788. https://doi.org/10.1126/science.aan2788.
[4] Liu P, de la Vega MR, Dodson M, Yue F, Shi B, Fang D, Chapman E, Liu L, Zhang DD. Spermidine confers liver protection by enhancing NRF2 signaling through a MAP1S-mediated noncanonical mechanism. Hepatology 2019;70(1):372–88. https://doi.org/10.1002/hep.30616.
[5] Ghosh I, Sankhe R, Mudgal J, Arora D, Nampoothiri M. News and Reviews Spermidine, an autophagy inducer, as a therapeutic strategy in neurological disorders. Neuropeptides 2020;83:102083. https://doi.org/10.1016/j.npep.2020.102083.
[6] Zimmermann A, Carmona-Gutierrez D, Madeo F. Spermidine supplementation in rare translation-associated disorders. Cell Stress 2021;5(3):29–32. https://doi.org/10.15698/cst2021.03.243.
[7] Ma L, Ni Y, Hu L, Zhao Y, Zheng L, Yang S, Ni L, Fu Z. Spermidine ameliorates high-fat diet-induced hepatic steatosis and adipose tissue inflammation in preexisting obese mice. Life Sci 2021;265:118739. https://doi.org/10.1016/j.lfs.2020.118739.
[8] Qin J, Krivoruchko A, Ji B, Chen Y, Kristensen M, Özdemir E, Keasling JD, Jensen MK, Nielsen J. Engineering yeast metabolism for the discovery and production of polyamines and polyamine analogues. Nat Catal 2021;4(6):498–509. https://doi.org/10.1038/s41929-021-00631-z.
[9] Liu Y, Guo X, Wang X, Chen K, Ouyang P. A two-enzyme cascade system for the bio-production of spermidine from putrescine. Mol Catal 2021;504:111439. https://doi.org/10.1016/j.mcat.2021.111439.
[10] Zou D, Li L, Min Y, Ji A, Liu Y, Wei X, Wang J, Wen Z. Biosynthesis of a novel bioactive metabolite of spermidine from *Bacillus amyloliquefaciens*: gene mining, sequence analysis, and combined expression. J Agric Food Chem 2021;69(1):267–74. https://doi.org/10.1021/acs.jafc.0c07143.
[11] Kim SK, Jo JH, Park YC, Jin YS, Seo JH. Metabolic engineering of *Saccharomyces cerevisiae* for production of spermidine under optimal culture conditions. Enzym Microb Technol 2017;101:30–5. https://doi.org/10.1016/j.enzmictec.2017.03.008.
[12] Tait GH. The formation of homospermidine by an enzyme from *Rhodopseudomonas viridis*. Biochem Soc Trans 1979;7(1):199–201.
[13] Ober D, Tholl D, Martin W, Hartmann T. Homospermidine synthase of *Rhodopseudomonas viridis*: substrate specificity and effects of the heterologously expressed enzyme on polyamine metabolism of *Escherichia coli*. J Gen Appl Microbiol 1996;42(5):411–9. https://doi.org/10.2323/jgam.42.411.
[14] Zhou X-J, Wang M-Y, Zhao L, He Y-Q, Wang Z-Q, Li J-J, Deng G-Z, Wan N-W, Chen Y-Z. Enantiodivergent synthesis of halohydrins by engineering P450DA monooxygenases. ACS Catal 2023:15948–55. https://doi.org/10.1021/acscatal.3c04742.
[15] Yeo WL, Tay DWP, Miyajima JMT, Supekar S, Teh TM, Xu J, Tan YL, See JY, Fan H, Maurer-Stroh S, Lim YH, Ang EL. Directed evolution and computational modeling of galactose oxidase toward bulky benzylic and alkyl secondary alcohols. ACS Catal 2023:16088–96. https://doi.org/10.1021/acscatal.3c03427.
[16] Wu H, Yi M, Wu X, Ding Y, Pu M, Wen L, Cheng Y, Zhang W, Mu W. Engineering the thermostability of d-lyxose isomerase from Caldanaerobius polysaccharolyticus via multiple computer-aided rational design for efficient synthesis of d-mannose. Synth Syst Biotechnol 2023;8(2):323–30. https://doi.org/10.1016/j.synbio.2023.04.003.
[17] Krossa S, Faust A, Ober D, Scheidig AJ. Comprehensive structural characterization of the bacterial homospermidine synthase-an essential enzyme of the polyamine metabolism. Sci Rep 2016;6:19501. https://doi.org/10.1038/srep19501.
[18] Helfrich F, Scheidig AJ. Structural and catalytic characterization of *Blastochloris viridis* and *Pseudomonas aeruginosa* homospermidine synthases supports the essential role of cation-pi interaction. Acta Crystallogr D Struct Biol 2021;77(Pt 10):1317–35. https://doi.org/10.1107/S2059798321008937.
[19] Wachtmeister J, Rother D. Recent advances in whole cell biocatalysis techniques bridging from investigative to industrial scale. Curr Opin Biotechnol 2016;42:169–77. https://doi.org/10.1016/j.copbio.2016.05.005.
[20] Schultes FPJ, Haarmann M, Tischler D, Mügge C. Primary alcohols as substrates or products in whole-cell biocatalysis: toxicity for Escherichia coli expression strains. Mol Catal 2023;538. https://doi.org/10.1016/j.mcat.2023.112979.
[21] Lin B, Tao Y. Whole-cell biocatalysts by design. Microb Cell Factories 2017;16(1). https://doi.org/10.1186/s12934-017-0724-7.
[22] Liu H, Wei W, Pang Z, Gu S, Song W, Gao C, Chen X, Liu J, Guo L, Wu J, Liu L. Protein engineering, cofactor engineering, and surface display engineering to achieve whole-cell catalytic production of chondroitin sulfate A. Biotechnol Bioeng 2023;120(7):1784–96. https://doi.org/10.1002/bit.28423.
[23] Schelch S, Eibinger M, Zuson J, Kuballa J, Nidetzky B. Modular bioengineering of whole-cell catalysis for sialo-oligosaccharide production: coordinated co-expression of CMP-sialic acid synthetase and sialyltransferase. Microb Cell Factories 2023;22(1). https://doi.org/10.1186/s12934-023-02249-1.
[24] Liang X, Deng H, Bai Y, Fan TP, Zheng X, Cai Y. Highly efficient biosynthesis of spermidine from L-homoserine and putrescine using an engineered *Escherichia coli* with NADPH self-sufficient system. Appl Microbiol Biotechnol 2022;106(17):5479–93. https://doi.org/10.1007/s00253-022-12110-x.
[25] Liu W, Hu X, Fang L, Cai Y. Insights into the unusual activity of a novel homospermidine synthase with a promising application to produce spermidine. J Agric Food Chem 2023;71(35):13024–34. https://doi.org/10.1021/acs.jafc.3c03037.
[26] Wang X, Nie Y, Mu X, Xu Y, Xiao R. Disorder prediction-based construct optimization improves activity and catalytic efficiency of *Bacillus naganoensis* pullulanase. Sci Rep 2016;6. https://doi.org/10.1038/srep24574.
[27] Jumper J, Evans R, Pritzel A, Green T, Figurnov M, Ronneberger O, Tunyasuvunakool K, Bates R, Zidek A, Potapenko A, Bridgland A, Meyer C, Kohl SAA, Ballard AJ, Cowie A, Romera-Paredes B, Nikolov S, Jain R, Adler J, Back T, Petersen S, Reiman D, Clancy E, Zielinski M, Steinegger M, Pacholska M, Berghammer T, Bodenstein S, Silver D, Vinyals O, Senior AW, Kavukcuoglu K, Kohli P, Hassabis D. Highly accurate protein structure prediction with AlphaFold. Nature 2021;596(7873):583–9. https://doi.org/10.1038/s41586-021-03819-2.
[28] Trott O, Olson AJ. Software news and update AutoDock Vina: improving the speed and accuracy of docking with a new scoring function, efficient optimization, and multithreading. J Comput Chem 2010;31(2):455–61. https://doi.org/10.1002/jcc.21334.
[29] Lu C, Wu C, Ghoreishi D, Chen W, Wang L, Damm W, Ross GA, Dahlgren MK, Russell E, Von Bargen CD, Abel R, Friesner RA, Harder ED. OPLS4: improving force field accuracy on challenging regimes of chemical space. J Chem Theor Comput 2021;17(7):4291–300. https://doi.org/10.1021/acs.jctc.1c00302.
[30] Shaw DE, Maragakis P, Lindorff-Larsen K, Piana S, Dror RO, Eastwood MP, Bank JA, Jumper JM, Salmon JK, Shan Y, Wriggers W. Atomic-level characterization of the structural dynamics of proteins. Science 2010;330(6002):341–6. https://doi.org/10.1126/science.1187409.

[31] Smith BE, Wang SL, Jaime-Figueroa S, Harbin A, Wang J, Hamman BD, Crews CM. Differential PROTAC substrate specificity dictated by orientation of recruited E3 ligase. Nat Commun 2019;10(1):131. https://doi.org/10.1038/s41467-018-08027-7.

[32] Hu J, Chen X, Zhang L, Zhou J, Xu G, Ni Y. Engineering the thermostability of a d-carbamoylase based on ancestral sequence reconstruction for the efficient synthesis of d-tryptophan. J Agric Food Chem 2023;71(1):660–70. https://doi.org/10.1021/acs.jafc.2c07781.

[33] Shaw FL, Elliott KA, Kinch LN, Fuell C, Phillips MA, Michael AJ. Evolution and multifarious horizontal transfer of an alternative biosynthetic pathway for the alternative polyamine sym-homospermidine. J Biol Chem 2010;285(19):14711–23. https://doi.org/10.1074/jbc.M110.107219.

[34] Bottcher F, Adolph RD, Hartmann T. Homospermidine synthase, the first pathway-specific enzyme in pyrrolizidine alkaloid biosynthesis. Phytochemistry 1993;32(3):679–89. https://doi.org/10.1016/s0031-9422(00)95154-9.

[35] Guerra J, Ribeiro-Filho HV, Jara GE, Bortot LO, Pereira JGC, Lopes-de-Oliveira PS. pyKVFinder: an efficient and integrable Python package for biomolecular cavity detection and characterization in data science. BMC Bioinf 2021;22(1):607. https://doi.org/10.1186/s12859-021-04519-4.

[36] Martinez L. Automatic identification of mobile and rigid substructures in molecular dynamics simulations and fractional structural fluctuation analysis. PLoS One 2015;10(3):e0119264. https://doi.org/10.1371/journal.pone.0119264.

[37] Wang L, Diao S, Sun Y, Jiang S, Liu Y, Wang H, Wei D. Rational engineering of *Acinetobacter tandoii* glutamate dehydrogenase for asymmetric synthesis of l-homoalanine through biocatalytic cascades. Catal Sci Technol 2021;11(12):4208–15. https://doi.org/10.1039/d1cy00376c.

[38] Zou D, Zhao Z, Li L, Min Y, Zhang D, Ji A, Jiang C, Wei X, Wu X. A comprehensive review of spermidine: safety, health effects, absorption and metabolism, food materials evaluation, physical and chemical processing, and bioprocessing. Compr Rev Food Sci Food Saf 2022;21(3):2820–42. https://doi.org/10.1111/1541-4337.12963.

[39] Mindt M, Walter T, Kugler P, Wendisch VF. Microbial engineering for production of *N*-functionalized amino acids and amines. Biotechnol J 2020;15(7). https://doi.org/10.1002/biot.201900451.

[40] Hidese R, Toyoda M, Yoshino K-i, Fukuda W, Wihardja GA, Kimura S, Fujita J, Niitsu M, Oshima T, Imanaka T, Mizohata E, Fujiwara S. The C-terminal flexible region of branched-chain polyamine synthase facilitates substrate specificity and catalysis. FEBS J 2019;286(19):3926–40. https://doi.org/10.1111/febs.14949.

[41] Sekula B, Dauter Z. Crystal structure of thermospermine synthase from *Medicago truncatula* and substrate discriminatory features of plant aminopropyltransferases. Biochem J 2018;475:787–802. https://doi.org/10.1042/bcj20170900.

[42] Al-Attar S, Rendon J, Sidore M, Duneau J-P, Seduk F, Biaso F, Grimaldi S, Guigliarelli B, Magalon A. Gating of substrate access and long-range proton transfer in *Escherichia coli* nitrate reductase A: the essential role of a remote glutamate residue. ACS Catal 2021;11(23):14303–18. https://doi.org/10.1021/acscatal.1c03988.

[43] Rapp C, Nidetzky B. Hydride transfer mechanism of enzymatic sugar nucleotide C2 epimerization probed with a loose-fit CDP-glucose substrate. ACS Catal 2022;12(12):6816–30. https://doi.org/10.1021/acscatal.2c00257.